ACS Energy LETTERS

http://pubs.acs.org/journal/aelccp

Thin Solid Electrolyte Layers Enabled by Nanoscopic Polymer Binding

Yejing Li, Xuefeng Wang, Hongyao Zhou, Xing Xing, Abhik Banerjee, John Holoubek, Haodong Liu, Ying Shirley Meng, and Ping Liu*

Cite This: *ACS Energy Lett.* 2020, 5, 955–961

Read Online

ACCESS | Metrics & More | Article Recommendations | Supporting Information

ABSTRACT: To achieve high-energy all-solid-state batteries (ASSBs), solid-state electrolytes (SE) must be thin, mechanically robust, and possess the ability to form low resistance interfaces with electrode materials. Embedding an inorganic SE into an organic polymer combines the merits of high conductivity and flexibility. However, the performance of such an SE-in-polymer matrix (SEPM) is highly dependent on the microstructure and interactions between the organic and inorganic components. We report on the synthesis of a free-standing, ultrathin (60 μm) SEPM from a solution of lithium polysulfide, phosphorus sulfide, and ethylene sulfide (ES), where the polysulfide triggers the *in situ* polymerization of ES and the formation of Li_3PS_4. Reactant ratios were optimized to achieve a room-temperature conductivity of 2×10^{-5} S cm^{-1}. Cryogenic electron microscopy confirmed a uniform nanoscopic distribution of β-Li_3PS_4 and PES (polyethylene sulfide). This work presents a facile route to the scalable fabrication of ASSBs with promising cycling performance and low electrolyte loading.

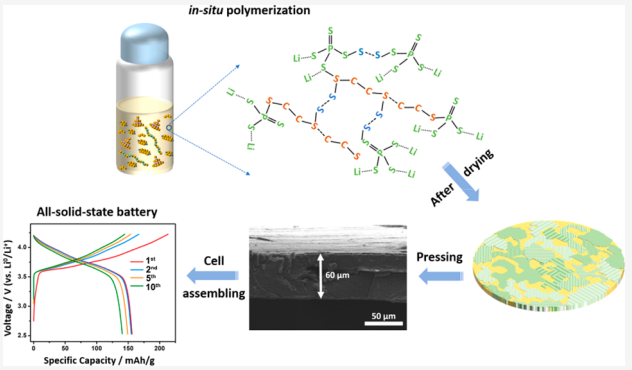

All-solid-state batteries (ASSBs) are being extensively studied as a next-generation energy-storage system because of their potential to provide high energy density and favorable safety properties.[1−4] In particular, solid-state electrolytes (SEs) promise to enable the utilization of Li metal as the anode, resulting in high energy density.[5] However, because of the difficulty of SE processing, large amounts of SE material are typically employed, resulting in a thick (up to 1 mm) electrolyte layer in lab-scale ASSBs, corresponding to a low practical energy density at the cell level.[6−9]

SE systems generally belong to one of two categories: oxide- or sulfide-based SEs, which possess distinct processing considerations due to their chemistry. Oxide-based SEs are stable in air but are brittle, requiring high-temperature sintering to reduce the grain boundary resistance. This sintering process often results in undesirable side reactions between the SE and electrode materials at the interface, which in turn produces a high charge-transfer resistance. Furthermore, the low processability of oxide-based SEs requires costly and time-consuming fabrication strategies to reduce SE thickness, such as pulsed laser deposition (PLD),[10] physical vapor deposition (PVD),[11] and chemical vapor deposition (CVD).[12] By contrast, sulfide-based SEs are quite deformable and can be densified at room temperature via cold-pressing, indicating their promise to generate a favorable interface with electrode materials.[13] Despite this, it is still difficult to achieve a thin and dense SE pellet during ASSB fabrication without any cracks and voids regardless of the pressure applied during densification. As a result, the obtained SE pellet is usually as thick as hundreds of micrometers with relatively high porosity.[14,15] The presence of such porosity in the SE pellet serves as a pathway for Li dendrites to penetrate through the SE and short the ASSBs. Therefore, it is critical to develop a versatile approach to prepare thin and dense SE films for achieving practical high-energy ASSBs.

To achieve a thin and dense ASSB, a polymer binder is often introduced into the inorganic SE, termed a solid electrolyte-in-polymer matrix (SEPM). In principle, this SEPM would reduce the porosity of the SE film, enhance its mechanical properties, and improve physical contact with the electrode materials. The performance of this SEPM system is known to be dependent on the microstructure and the distribution of inorganic and polymer domains, which are all defined by the applied

Received: January 7, 2020
Accepted: February 26, 2020
Published: February 26, 2020

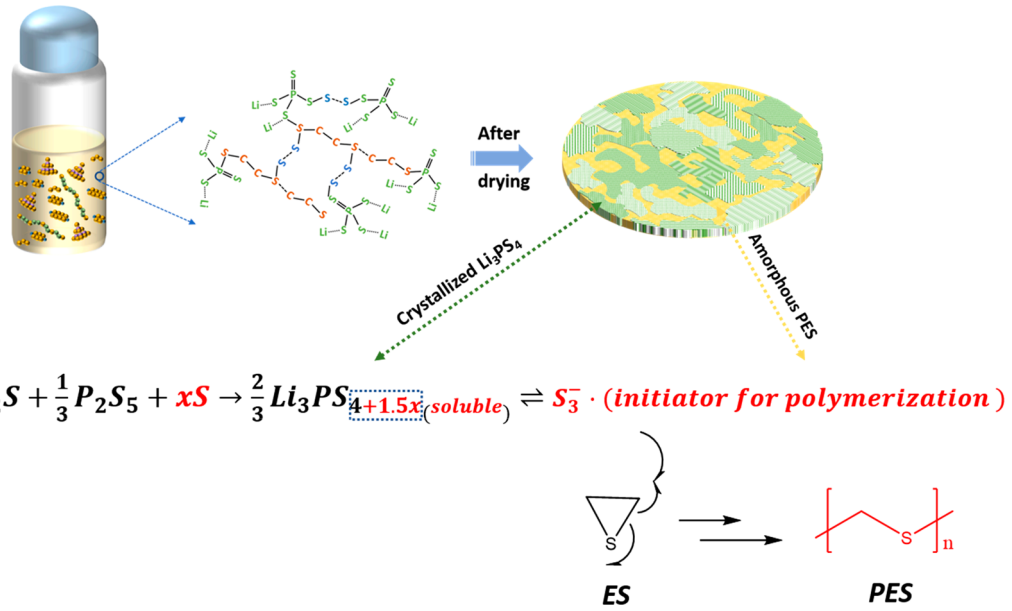

Figure 1. Schematic images for β-Li_3PS_4-S-PES synthesis and its structure.

synthesis method. At present, the most common methods of synthesizing SEPM is the physical mixing of inorganic and organic components in an inert solvent followed by casting.[16] Of note, Lee and co-workers[17] reported an SE in a polymer matrix via the physical mixing of a monomer and the SE particles followed by mechanical compression. A polymer matrix was then formed by initiating the polymerization of the interstitial monomers in the SE, achieving a final relative density of 97%. Employing a microfabrication method, Kim and co-workers[18] demonstrated a flexible Li-ion-conducting membrane, wherein a single layer of Li-ion-conducting ceramic particles were embedded in a polymer matrix. The as-prepared membrane was found to be as thin as 100 μm and possessed a high ionic conductivity. It is important to note that despite this progress, the development of more scalable methods for SEPM fabrication is still required to enable practical ASSBs at a commercial scale.

An ideal SEPM should feature the mechanical flexibility of the polymer matrix, strong interactions at the polymer/electrolyte interface to avoid delamination, a small electrolyte domain size to mitigate fracture, and a three-dimensional continuous pathway to achieve high ionic conductivity. In this regard, a nanocomposite bicontinuous structure would be highly desirable; however, realizing such a structure using physical mixing is not possible. In contrast, we propose that a scalable solution-based process whereby both domains can be formed from soluble precursors is a promising approach. Such a solution method would also enable the deposition of SEPM directly onto the surface of electrodes to form intimate interfacial contacts with low resistance. Solution-based methods are also known to provide other advantages, such as facile processing at low temperatures.[19−24] Our group recently obtained an ultrathin, dense, and homogeneous sulfide-based SE on Li metal and achieved promising electrochemical performance using such a method.[25]

In this work, we report the solution synthesis of a solid electrolyte-in-polymer matrix (SEPM) with potential chemical interactions between the inorganic and polymeric nanodomains via an *in situ* polymerization reaction. β-Li_3PS_4 was selected as the inorganic SE because of its higher ionic conductivity than typical oxide-based SEs.[1,3,26,27] Polyethylene sulfide (PES) was then *in situ* polymerized in this SE matrix, forming bonds with the β-Li_3PS_4 via polysulfide phases, resulting in a β-Li_3PS_4-S-PES nanocomposite. Cryogenic transmission electron microscopy (Cryo-TEM) and scanning TEM/energy dispersive X-ray spectroscopy confirm the nanoscopic distribution of the inorganic SEs and polymer matrix, yielding an ionic conductivity of 2.91×10^{-5} S cm^{-1} at room temperature after compositional optimization. With the aid of a nonwoven scaffold, we demonstrated a bendable and ultrathin SE which enables excellent electrochemical performance of ASSBs. Our approach provides a new scalable direction for the design and facile synthesis of thin, dense, and flexible solid electrolytes with high ionic conductivity and low interfacial resistance for practical solid-state batteries.

Synthesis of the Solid Electrolyte-in-Polymer Matrix. Figures 1 and S1 show the schematics of the synthesis approach for the SEPM β-Li_3PS_4-S-PES. Tetrahydrofuran (THF) was selected as the solvent stemming from our previous work, which demonstrated that β-Li_3PS_4 could be formed from the solvent solution and that ES was also soluble in THF for the purposes of the SEPM.[25] Li_2S and sulfur (S) were dissolved followed by the addition of stoichiometric ratio of P_2S_5/Li_2S = 1/3, forming a Li_3PS_{4+x} (x = 2, 1.6, and 1.2) solution. The color of the solution was brown, the shade of which varied depending on the concentration of the constituents (Figure S2). On the basis of the color alone, we believe there is formation of polysulfides such as S^{3-} radical as well other species of polysulfides because of the known disproportionation reaction of polysulfides.[28,29] The above solution was then combined with a second ES/THF solution to initiate the *in situ* polymerization between Li_3PS_{4+x} and PES triggered by residual S_3^- radicals produced by the P_2S_5/Li_2S dissolution, at which point a change of solution color was observed. After THF removal, a solid SEPM Li_3PS_{4+x}-PES or Li_3PS_4-S-PES was obtained.

To obtain an SEPM with high ion conductivity, we found that it was necessary to tune the content ratio of β-Li_3PS_4, S, and PES. First, the PES content was controlled by varying the amount of ES from 0.75, 1.5, to 3.0 mmol while the molar ratio

https://dx.doi.org/10.1021/acsenergylett.0c00040
ACS Energy Lett. 2020, 5, 955−961

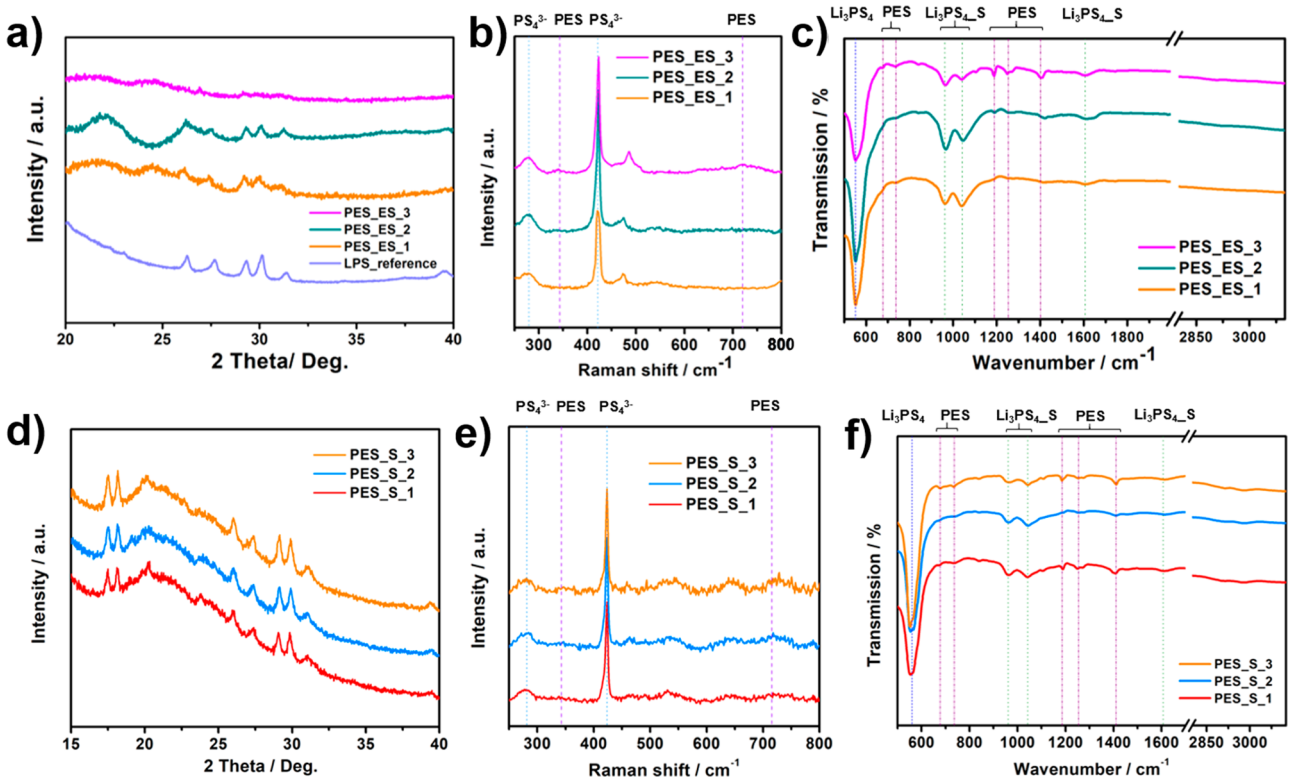

Figure 2. XRD (a and d), Raman (b and e), and FTIR (c and f) spectra of the SEPM with varying PES content (a–c) and S content (d–f).

of S/Li_2S was fixed to 2 (see details in Table S1). The corresponding samples are denoted as PES_ES_x (x = 1, 2, and 3 correspond to 0.75, 1.5, and 3.0 mmol for ES, respectively) and characterized by XRD, Raman, and Fourier transform infrared spectroscopy (FTIR). The XRD results (Figure 2a) show that with increasing PES content, the signal from the crystalline Li_3PS_4 phase becomes weaker, indicating that there are likely interactions between the Li_3PS_4 and PES, resulting in a nanoscale dispersion of crystalline domains. Note that pure PES is amorphous, as no obvious XRD signal from the PES was found. Raman, FTIR, and X-ray photoelectron spectroscopy (XPS) were carried out to further investigate the chemical structure of the SEPM (Figures 2b,c, S3, and S4). The strong peak at the Raman shift of 421 cm^{-1} is known to be the characteristic vibration of $\nu_s(PS_4)$, indicating the presence of the Li_3PS_4 in all the samples,[19] whereas the weak peaks at 340 and 724 cm^{-1} belong to δ(C–S–C) and ν_s(C–S) for PES, consistent with its characteristics peaks shown in Figure S3.[30] These two weak peaks slightly increased in intensity when more ES was added. It is worth mentioning that in addition to the peaks belonging to Li_3PS_4 and PES, a new peak is present in the Raman spectra of β-Li_3PS_4-S-PES at ~475 cm^{-1}, which can be assigned to polysulfides.[31] This peak was slightly blue-shifted when the ES content was increased, suggesting that polysulfides bridge the Li_3PS_4 and PES molecules. The presence of polysulfides and C–S bonds in the resultant SEPM was confirmed by the XPS as shown in Figure S4. FTIR results (Figure 2c) further corroborated the above explanations, in which characteristic peaks for PES, Li_3PS_4, and Li_3PS_4_S were identified. It was observed in the FTIR results that the PES peaks in the SEPM also display a slight blue shift at 672 and 724 cm^{-1} (Figure S3b),[30] compared to that of pure PES, which is further indication of the chemical bonding between the PES and Li_3PS_4_S. On the basis of the above information, we concluded that there is likely bonding at the interface of PES and Li_3PS_4 domains.

The ionic conductivity values of the SEPMs were measured by electrochemical impedance spectroscopy (EIS) at room temperature (Figure S5), where it was found that PES_ES_2 exhibited an optimal conductivity of 9.64 × 10^{-6} S cm^{-1}. In order to further increase the ionic conductivity of the β-Li_3PS_4-S-PES SEPM, attempts were made to reduce the amount of insulating S in the SEPM (Table S2). The resultant samples are denoted as PES_S_x (x = 1, 2, and 3, with the molar ratio of S/Li_2S as 2, 1.6, 1.2, respectively). Consistent with the above result, β-Li_3PS_4 is crystalline while PES and S are amorphous, and their presence was confirmed by the XRD pattern, Raman, and FTIR results shown in Figure 2d–f. It is noteworthy that it is difficult to clarify the formation of the polymorphs in the obtained samples because of the relative low intensity of the diffraction signals. Nevertheless, no peaks for $P_2S_6^{2-}$ (395 cm^{-1}), $P_2S_6^{4-}$ (382 cm^{-1}), and $P_2S_7^{4-}$ (406 cm^{-1}) species were found in the zoomed-in region of the Raman spectra of the SEPM composite with different ES and S content in Figure S6, confirming the dominance of the β-Li_3PS_4 phase. Therefore, slightly reducing the S content was found to increase the ionic conductivity of the β-Li_3PS_4-S-PES SEPM without altering the chemical or physical structure. The SEPM with the S/Li_2S ratio of 1.6 resulted in the highest ionic conductivity of 2.03 × 10^{-5} S cm^{-1} at room temperature, whereas the lower conductivities of SEPMs with S/Li_2S ratios of 1.2 and 2.0 are likely due to insufficient polysulfide connectivity between Li_3PS_4 and PES and the overabundance of insulating S, respectively. Thus, given the above analysis, the PES_S_2 sample was selected as the SEPM in the following characterizations and electrochemical tests. The Nyquist plot for PES_S_2 was fitted with the equivalent circuit shown in Figure S7. According to the EIS fitting, the resistance from the

https://dx.doi.org/10.1021/acsenergylett.0c00040
ACS Energy Lett. 2020, 5, 955–961

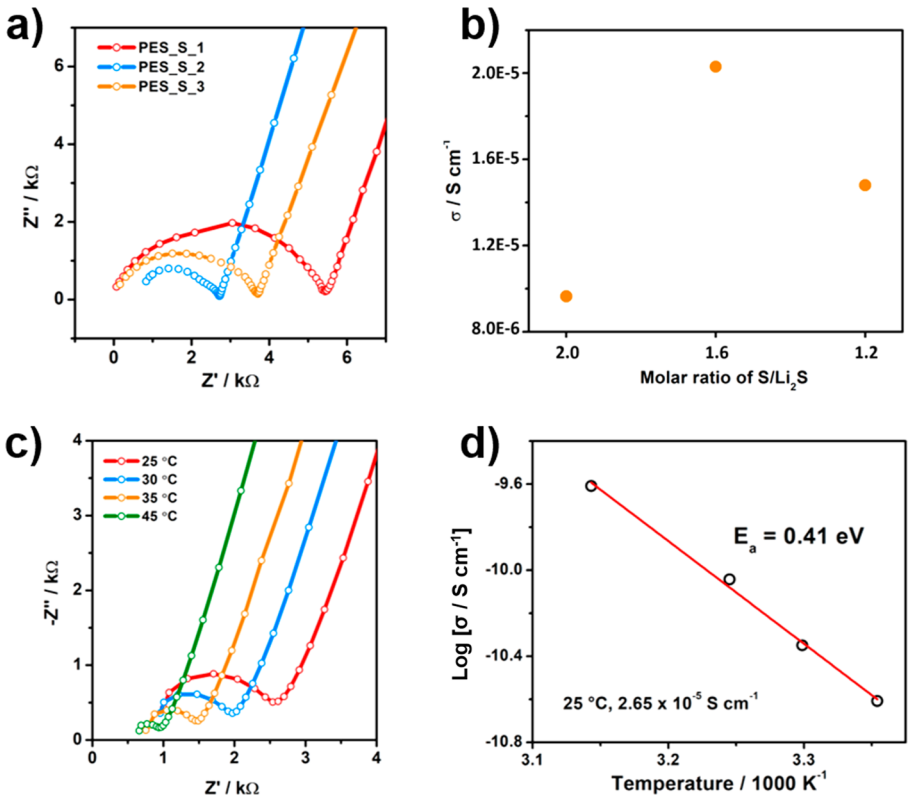

Figure 3. Nyquist plots (a) and the corresponding calculated ionic conductivity (b) for the SEPM with varying S content. Nyquist plots (c) at different temperatures and the corresponding Arrhenius plot (d) for PES_S_2. The additional bulk resistance in panel c compared with that in panel a is from the different instrument error and extra wire connection to the oven in the glovebox.

bulk is ~2366 Ω while that from the grain boundary is ~353 Ω, indicating that the ionic transport in the SE is dominated by bulk resistance. The actual weight ratio of the β-Li_3PS_4, S, and PES in β-Li_3PS_4-S-PES SEPM was determined to be 65:15:20 by thermogravimetric analysis shown in Figure S8. The conductivity of the SEPM was also measured over a temperature range from 25 to 45 °C, and the activation energy was calculated to be 0.41 eV (Figure 3c,d), comparable to that of bulk β-Li_3PS_4 (0.47 eV), which agrees with reported references summarized in Table S3. The ionic conductivity of the SEPM at temperature extremes of of −15 and 65 °C were also measured to be 2.51×10^{-6} S cm^{-1} (Figure S9) and 1.29×10^{-4} S cm^{-1} (Figure S10), respectively.

Potential Interaction between Inorganic and Organic Domains. To unravel the effect of microstructure on the ionic conductivity of the β-Li_3PS_4-S-PES SEPM, its morphology and nanostructure were examined by SEM and cryogenic TEM. For comparison, a mixture of β-Li_3PS_4, S, and PES was prepared by physical blending, which yielded an ionic conductivity of 1.28×10^{-6} S cm^{-1} (Figure S12). As shown in Figure S11, all of the particles in the *in situ*-formed composite are almost identical (Figure S11a,b), while those in the physically blended mixture are clearly distinguishable and show distinct morphologies for the different SE components (Figure S11c,d). This indicates that β-Li_3PS_4, S, and PES are evenly distributed in the *in situ*-formed β-Li_3PS_4-S-PES with intimate particle contact beyond the detection capability of SEM, whereas the contact between the different species in the physically blended mixture is easily detectable and therefore insufficient. Hence, we conclude that the discrepancy in ionic conductivity stems from the homogeneous nanoscale distribution of organic and inorganic SEPM constituents.

In order to visualize the distribution of the PES, S, and Li_3PS_4 at the nano scale (Figure 4a), scanning transmission electron microscopy−energy dispersive spectroscopy (STEM-EDS) was conducted under cryogenic protection, which is essential to reducing beam damage to the SEPM.[32] The distribution of carbon (C), sulfur (S), and phosphorus (P) is shown in Figure 4b−d. Because C and P originate solely from the PES and Li_3PS_4, they can be used to represent and distinguish the PES and Li_3PS_4, respectively, revealing an extremely uniform distribution at the nanoscale with no visible elemental aggregation.

To further reveal the nanostructure of the β-Li_3PS_4-S-PES SEPM, cryogenic high-resolution TEM (cryo-HRTEM) was employed. Consistent with the above SEM and EDS results, the SEPM displays a uniform and fully integrated structure (Figure 4e), which consisted of many crystalline and amorphous nanodomains (Figure 4f). By the fast Fourier transformation (FFT) of Figure 4e, polycrystalline rings (inset in Figure 4e) can be indexed to the Li_3PS_4, which is consistent with XRD results. The absence of characteristic diffraction patterns of PES and S further confirms their amorphous nature. These crystalline Li_3PS_4 nanodomains display an average size of roughly 5 nm and are observed to be embedded into the PES-S polymer matrix. Combined with the above cryo-STEM-EDS results, we conclude that an even distribution of the organic and inorganic species at a nano scale was obtained via the solution-based *in situ* polymerization method.

Freestanding SEPM@Kevlar Film Fabrication. With the prepared β-Li_3PS_4-S-PES SEPM nanocomposite, we then

https://dx.doi.org/10.1021/acsenergylett.0c00040
ACS Energy Lett. 2020, 5, 955−961

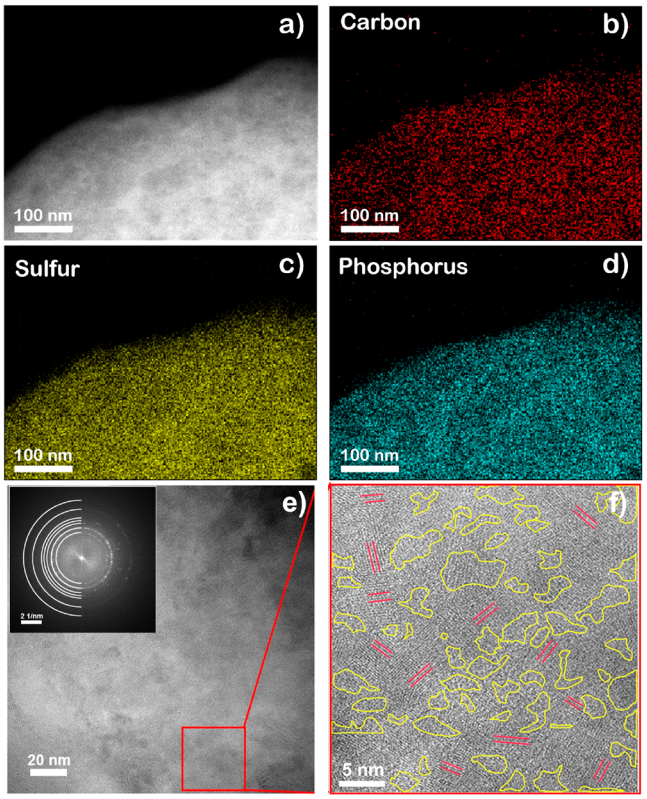

Figure 4. Cryo-STEM (a) and cryo-STEM-EDS (panels b, c, and d represent for the elemental mapping of C, S, and P, respectively) for the as-prepared SEPM. Cryo-TEM (e and f) and the corresponding FFT images (inset in panel e) for the as-prepared SEPM. Areas with yellow circles and red lines correspond to the amorphous and crystalline species, respectively.

fabricated a thin, dense, and flexible SE supported by a Kevlar mat, the addition of which (Figure 5a) has been previously

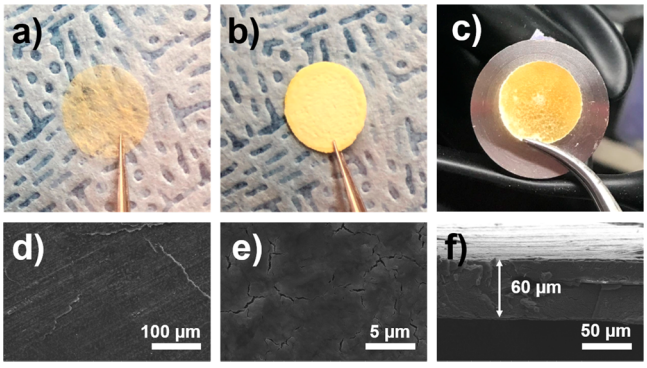

Figure 5. Images for the original Kevlar mat (a), dried SEPM@Kevlar pellet (b), and the pressed dried SEPM@Kevlar film (c). Panels d–f are the corresponding SEM images of the top view and cross section of the pressed dried SEPM@Kevlar film.

found to further enhance the mechanical properties of SE films without sacrificing ionic conductivity (Figure S13).[23] This integration was achieved by dropping Li_3PS_4_S_PES onto the Kevlar mat (Figure 5a), followed by the removal of residual solvent, yielding an ultrathin SEPM@Kevlar film (Figure 5b). The SEPM@Kevlar film was also found to be remarkably flexible, as shown in Video S1. The thickness of the electrolyte membrane can be tuned by controlling the volume of the Li_3PS_4_S_PES solution. A 60 μm thickness SEPM@Kevlar film was achieved in this regard with a very smooth and dense surface (Figure 5c–f) at an estimated porosity of 5.6% (see detailed calculations in the Supporting Information), demonstrating the promise of this SEPM@Kevlar film fabrication method toward practical high-energy all-solid-state batteries.

Electrochemical Test. The electrochemical performance of the ultrathin free-standing SEPM was first evaluated in Li–In||SEPM||Li–In symmetric cells at 60 °C as displayed in Figure 6a. The applied current was 0.5 mA cm^{-2}, and the capacity for each stripping/plating was 0.25 mAh cm^{-2}, that is, 0.05 mg Li, and yields stable and flat voltage plateaus during repeated cycling. The overpotential was found to be about 100 mV and remained stable over the duration of the test. The cell was able to run as long as 106 h without any shorting, despite the low thickness of the prepared SEPM. With continuous cycling, sharp peaks began appear at the end of the charge and discharging process, which may be attributable to insufficient Li in the $Li_{0.5}In$ alloy, leading to the sluggish diffusion of Li ions.[33]

The ultrathin free-standing SEPM was then applied in a full-cell, where a Li–In alloy and $LiNbO_3$ coated Li-$Ni_{0.80}Co_{0.15}Al_{0.05}O_2$ (LNO-NCA) were employed as the anode and cathode, respectively (Figure 6b,c). Of note, the $LiNbO_3$ coating has been commonly applied to mitigate reactions between NCA and Li_3PS_4.[34,35] This cell was cycled at 60 °C between 2.5 and 4.2 V at a current density of 18 mA g^{-1}, producing an initial reversible capacity of 156.3 mAh g^{-1}, and retained 81.2% of its capacity after 20 cycles. The capacity from OCV to 3.5 V during the initial charge process can be attributed to the side reactions between the LNO-NCA and the SEPM, which disappears in the following cycle, indicating that this side reaction was subsequently inhibited. Rate tests (Figure 6c) demonstrate a 1*C* capacity of 33 mAh/g which recovered to 121.6 mAh/g when the rate returned to *C*/15. The gradual capacity degradation may be caused by the side reaction between SEPM and NCA at high temperature, which will be a subject of further investigation moving forward.

We have developed a novel synthesis method for nanocomposite solid electrolyte-in-polymer matrices (SEPM) based on the *in situ* free-radical polymerization of PES inside of a Li_3PS_{4+x} solution. This *in situ* polymerization reaction produces an SEPM with intimate contact between the crystalline and polymer species and was optimized for ionic conductivity by tuning the content of the S and ES, yielding an SEPM with an ionic conductivity of 2.5×10^{-5} S cm^{-1} at room temperature. XRD, Raman, and FTIR results confirm the coexistence of the crystallized Li_3PS_4 and amorphous PES in addition to cryo-TEM and cryo-STEM/EDX results, which showed that the Li_3PS_4 and PES domains form a nanocomposite with domain sizes of a few nanometers. The nanoscopic distribution of the organic and inorganic species was found to enable high ionic conductivity despite the inclusion of insulating S and PES into the solid-state electrolyte. From a solution precursor, an ultrathin 60 μm free-standing electrolyte was fabricated and applied in a solid-state battery utilizing an LNO–NCA cathode and Li–In alloy anode, which delivered a cathode capacity of 156.3 mAh/g. Our approach demonstrates the great promise of *in situ* solution synthesis methods for the formation of nanocomposite electrolytes that are thin, mechanically robust, and conductive, all attributes essential to enable practical all-solid-state batteries. This work represents a synthesis approach

https://dx.doi.org/10.1021/acsenergylett.0c00040
ACS Energy Lett. 2020, 5, 955–961

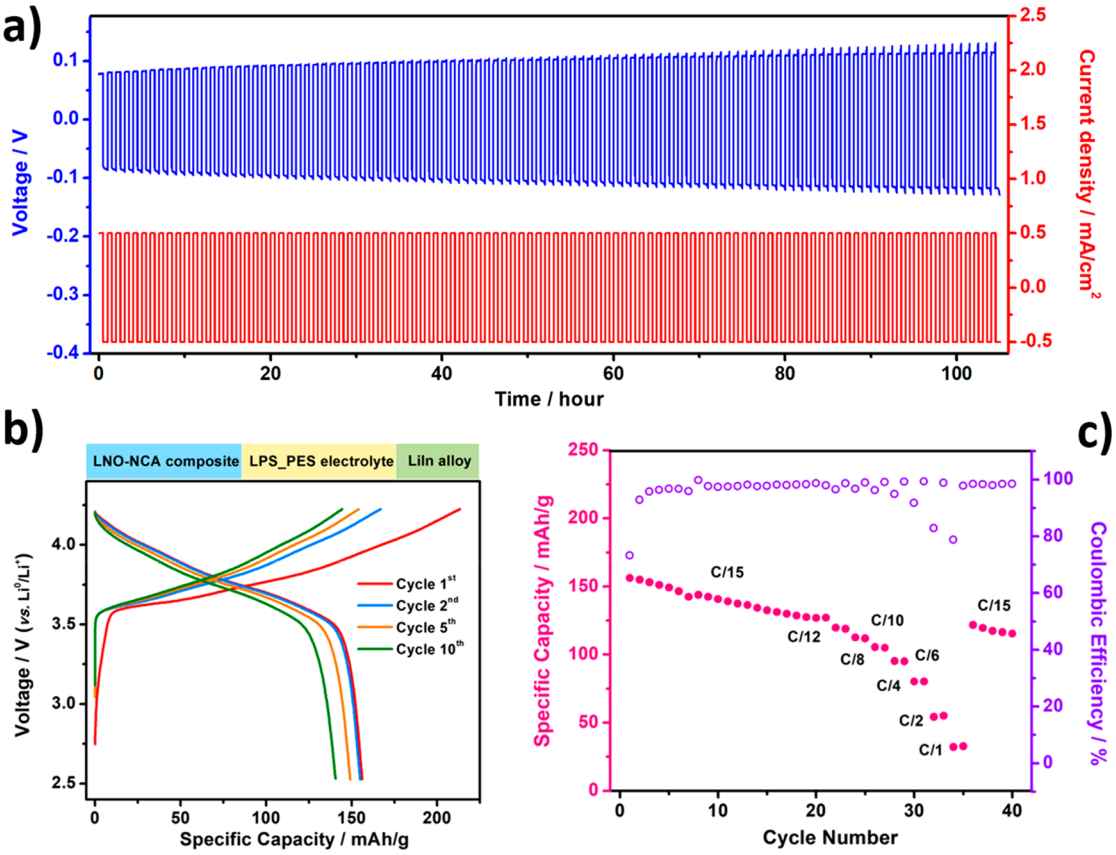

Figure 6. Galvanostatic cycling of the Li−In||SEPM||Li−In symmetric cell (a). Voltage profiles (b) and rate performance (c) of the Li−In|| SEPM||LNO-NCA composite full cell. All cells are tested under 60 °C.

to achieve easily processable, thin, mechanically stable solid electrolyte layers with high performance.

■ ASSOCIATED CONTENT

Supporting Information

The Supporting Information is available free of charge at https://pubs.acs.org/doi/10.1021/acsenergylett.0c00040.

Additional experimental, characterizations, electrochemical test and calculation details, figures showing Raman, FTIR, thermogravimetric analysis, SEM of the as-prepared samples and Nyquist plots, tables for synthesis of the samples and summary of the activation energy for related electrolyte from the references (PDF)

Video S1: flexible SEPM@Kevlar film (MP4)

■ AUTHOR INFORMATION

Corresponding Author

Ping Liu − *Department of NanoEngineering, University of California San Diego, La Jolla, California 92093, United States; Sustainable Power and Energy Center, University of California, San Diego, La Jolla, California 92093, United States;* orcid.org/0000-0002-1488-1668; Email: piliu@eng.ucsd.edu

Authors

Yejing Li − *Department of NanoEngineering, University of California San Diego, La Jolla, California 92093, United States*

Xuefeng Wang − *Department of NanoEngineering, University of California San Diego, La Jolla, California 92093, United States*

Hongyao Zhou − *Department of NanoEngineering, University of California San Diego, La Jolla, California 92093, United States*

Xing Xing − *Department of NanoEngineering, University of California San Diego, La Jolla, California 92093, United States*

Abhik Banerjee − *Department of NanoEngineering, University of California San Diego, La Jolla, California 92093, United States*

John Holoubek − *Department of NanoEngineering, University of California San Diego, La Jolla, California 92093, United States*

Haodong Liu − *Department of NanoEngineering, University of California San Diego, La Jolla, California 92093, United States*

Ying Shirley Meng − *Department of NanoEngineering, University of California San Diego, La Jolla, California 92093, United States; Sustainable Power and Energy Center, University of California, San Diego, La Jolla, California 92093, United States;* orcid.org/0000-0001-8936-8845

Complete contact information is available at: https://pubs.acs.org/10.1021/acsenergylett.0c00040

Notes

The authors declare no competing financial interest.

■ ACKNOWLEDGMENTS

This work has been supported by the Advanced Research Projects Agency-Energy, U.S. Department of Energy, under Contract No. DE-AR0000781. TEM was performed at the University of California, Irvine Materials Research Institute (IMRI) using instrumentation funded in part by the National Science Foundation Major Research Instrumentation Program

https://dx.doi.org/10.1021/acsenergylett.0c00040
ACS Energy Lett. 2020, 5, 955−961

under Grant CHE-1338173. Y.S.M. acknowledges the Zable Endowed Chair in Energy Technologies fund.

REFERENCES

(1) Manthiram, A.; Yu, X.; Wang, S. Lithium battery chemistries enabled by solid-state electrolytes. *Nature Reviews Materials* **2017**, *2*, 16103.
(2) Xin, S.; You, Y.; Wang, S.; Gao, H.-C.; Yin, Y.-X.; Guo, Y.-G. Solid-State Lithium Metal Batteries Promoted by Nanotechnology: Progress and Prospects. *ACS Energy Letters* **2017**, *2* (6), 1385−1394.
(3) Hu, Y.-S. Batteries: Getting solid. *Nature Energy* **2016**, *1*, 16042.
(4) Sun, C.; Liu, J.; Gong, Y.; Wilkinson, D. P.; Zhang, J. Recent advances in all-solid-state rechargeable lithium batteries. *Nano Energy* **2017**, *33*, 363−386.
(5) Hallinan, D. T.; Villaluenga, I.; Balsara, N. P. Polymer and composite electrolytes. *MRS Bull.* **2018**, *43* (10), 759−767.
(6) Kamaya, N.; Homma, K.; Yamakawa, Y.; Hirayama, M.; Kanno, R.; Yonemura, M.; Kamiyama, T.; Kato, Y.; Hama, S.; Kawamoto, K.; Mitsui, A. A lithium superionic conductor. *Nat. Mater.* **2011**, *10* (9), 682−686.
(7) Yersak, T. A.; Macpherson, H. A.; Kim, S. C.; Le, V.-D.; Kang, C. S.; Son, S.-B.; Kim, Y.-H.; Trevey, J. E.; Oh, K. H.; Stoldt, C.; Lee, S.-H. Solid State Enabled Reversible Four Electron Storage. *Adv. Energy Mater.* **2013**, *3* (1), 120−127.
(8) Ohta, N.; Takada, K.; Zhang, L.; Ma, R.; Osada, M.; Sasaki, T. Enhancement of the High-Rate Capability of Solid-State Lithium Batteries by Nanoscale Interfacial Modification. *Adv. Mater.* **2006**, *18* (17), 2226−2229.
(9) van den Broek, J.; Afyon, S.; Rupp, J. L. M. Interface-Engineered All-Solid-State Li-Ion Batteries Based on Garnet-Type Fast Li +Conductors. *Adv. Energy Mater.* **2016**, *6* (19), 1600736.
(10) Reinacher, J.; Berendts, S.; Janek, J. Preparation and electrical properties of garnet-type Li6BaLa2Ta2O12 lithium solid electrolyte thin films prepared by pulsed laser deposition. *Solid State Ionics* **2014**, *258*, 1−7.
(11) Yada, C.; Lee, C. E.; Laughman, D.; Hannah, L.; Iba, H.; Hayden, B. E. A High-Throughput Approach Developing Lithium-Niobium-Tantalum Oxides as Electrolyte/Cathode Interlayers for High-Voltage All-Solid-State Lithium Batteries. *J. Electrochem. Soc.* **2015**, *162* (4), A722−A726.
(12) Loho, C.; Djenadic, R.; Bruns, M.; Clemens, O.; Hahn, H. Garnet-Type Li7La3Zr2O12 Solid Electrolyte Thin Films Grown by CO2-Laser Assisted CVD for All-Solid-State Batteries. *J. Electrochem. Soc.* **2017**, *164* (1), A6131−A6139.
(13) Choi, S.; Ann, J.; Do, J.; Lim, S.; Park, C.; Shin, D. Application of Rod-Like Li6PS5Cl Directly Synthesized by a Liquid Phase Process to Sheet-Type Electrodes for All-Solid-State Lithium Batteries. *J. Electrochem. Soc.* **2019**, *166* (3), A5193−A5200.
(14) Kim, A. Y.; Strauss, F.; Bartsch, T.; Teo, J. H.; Hatsukade, T.; Mazilkin, A.; Janek, J.; Hartmann, P.; Brezesinski, T. Stabilizing Effect of a Hybrid Surface Coating on a Ni-Rich NCM Cathode Material in All-Solid-State Batteries. *Chem. Mater.* **2019**, *31* (23), 9664−9672.
(15) Santhosha, A. L.; Nayak, P. K.; Pollok, K.; Langenhorst, F.; Adelhelm, P. Exfoliated MoS2 as Electrode for All-Solid-State Rechargeable Lithium-Ion Batteries. *J. Phys. Chem. C* **2019**, *123* (19), 12126−12134.
(16) Xu, H.; Chien, P.-H.; Shi, J.; Li, Y.; Wu, N.; Liu, Y.; Hu, Y.-Y.; Goodenough, J. B. High-performance all-solid-state batteries enabled by salt bonding to perovskite in poly(ethylene oxide). *Proc. Natl. Acad. Sci. U. S. A.* **2019**, *116* (38), 18815−18821.
(17) Whiteley, J. M.; Taynton, P.; Zhang, W.; Lee, S.-H. Ultra-thin Solid-State Li-Ion Electrolyte Membrane Facilitated by a Self-Healing Polymer Matrix. *Adv. Mater.* **2015**, *27* (43), 6922−6927.
(18) Aetukuri, N. B.; Kitajima, S.; Jung, E.; Thompson, L. E.; Virwani, K.; Reich, M.-L.; Kunze, M.; Schneider, M.; Schmidbauer, W.; Wilcke, W. W.; Bethune, D. S.; Scott, J. C.; Miller, R. D.; Kim, H.-C. Flexible Ion-Conducting Composite Membranes for Lithium Batteries. *Adv. Energy Mater.* **2015**, *5* (14), 1500265.
(19) Liu, Z.; Fu, W.; Payzant, E. A.; Yu, X.; Wu, Z.; Dudney, N. J.; Kiggans, J.; Hong, K.; Rondinone, A. J.; Liang, C. Anomalous High Ionic Conductivity of Nanoporous β-Li3PS4. *J. Am. Chem. Soc.* **2013**, *135* (3), 975−978.
(20) Lim, H.-D.; Yue, X.; Xing, X.; Petrova, V.; Gonzalez, M.; Liu, H.; Liu, P. Designing solution chemistries for the low-temperature synthesis of sulfide-based solid electrolytes. *J. Mater. Chem. A* **2018**, *6* (17), 7370−7374.
(21) Pang, Q.; Liang, X.; Shyamsunder, A.; Nazar, L. F. An In Vivo Formed Solid Electrolyte Surface Layer Enables Stable Plating of Li Metal. *Joule* **2017**, *1* (4), 871−886.
(22) Zhou, L.; Park, K.-H.; Sun, X.; Lalère, F.; Adermann, T.; Hartmann, P.; Nazar, L. F. Solvent-Engineered Design of Argyrodite Li6PS5X (X = Cl, Br, I) Solid Electrolytes with High Ionic Conductivity. *ACS Energy Letters* **2019**, *4* (1), 265−270.
(23) Nam, Y. J.; Cho, S.-J.; Oh, D. Y.; Lim, J.-M.; Kim, S. Y.; Song, J. H.; Lee, Y.-G.; Lee, S.-Y.; Jung, Y. S. Bendable and Thin Sulfide Solid Electrolyte Film: A New Electrolyte Opportunity for Free-Standing and Stackable High-Energy All-Solid-State Lithium-Ion Batteries. *Nano Lett.* **2015**, *15* (5), 3317−3323.
(24) Oh, D. Y.; Kim, D. H.; Jung, S. H.; Han, J. G.; Choi, N. S.; Jung, Y. S. Single-step wet-chemical fabrication of sheet-type electrodes from solid-electrolyte precursors for all-solid-state lithium-ion batteries. *J. Mater. Chem. A* **2017**, *5* (39), 20771−20779.
(25) Lim, H.-D.; Lim, H.-K.; Xing, X.; Lee, B.-S.; Liu, H.; Coaty, C.; Kim, H.; Liu, P. Solid Electrolyte Layers by Solution Deposition. *Adv. Mater. Interfaces* **2018**, *5* (8), 1701328.
(26) Kato, Y.; Hori, S.; Saito, T.; Suzuki, K.; Hirayama, M.; Mitsui, A.; Yonemura, M.; Iba, H.; Kanno, R. High-power all-solid-state batteries using sulfide superionic conductors. *Nature Energy* **2016**, *1*, 16030.
(27) Janek, J.; Zeier, W. G. A solid future for battery development. *Nature Energy* **2016**, *1*, 16141.
(28) Pickering, T. L.; Saunders, K. J.; Tobolsky, A. V. Disproportionation of organic polysulfides. *J. Am. Chem. Soc.* **1967**, *89* (10), 2364−2367.
(29) Ghidiu, M.; Ruhl, J.; Culver, S. P.; Zeier, W. G. Solution-based synthesis of lithium thiophosphate superionic conductors for solid-state batteries: a chemistry perspective. *J. Mater. Chem. A* **2019**, *7* (30), 17735−17753.
(30) Angood, A. C.; Koenig, J. L. The laser-excited Raman spectra of polyethylene sulfide. *J. Macromol. Sci., Part B: Phys.* **1969**, *3* (2), 321−327.
(31) Hagen, M.; Schiffels, P.; Hammer, M.; Dörfler, S.; Tübke, J.; Hoffmann, M. J.; Althues, H.; Kaskel, S. In-Situ Raman Investigation of Polysulfide Formation in Li-S Cells. *J. Electrochem. Soc.* **2013**, *160* (8), A1205−A1214.
(32) Wang, X.; Li, Y.; Meng, Y. S. Cryogenic Electron Microscopy for Characterizing and Diagnosing Batteries. *Joule* **2018**, *2* (11), 2225−2234.
(33) Tan, D. H. S.; Wu, E. A.; Nguyen, H.; Chen, Z.; Marple, M. A. T.; Doux, J.-M.; Wang, X.; Yang, H.; Banerjee, A.; Meng, Y. S. Elucidating Reversible Electrochemical Redox of Li6PS5Cl Solid Electrolyte. *ACS Energy Letters* **2019**, *4* (10), 2418−2427.
(34) Culver, S. P.; Koerver, R.; Zeier, W. G.; Janek, J. On the Functionality of Coatings for Cathode Active Materials in Thiophosphate-Based All-Solid-State Batteries. *Adv. Energy Mater.* **2019**, *9* (24), 1900626.
(35) Li, X.; Jin, L.; Song, D.; Zhang, H.; Shi, X.; Wang, Z.; Zhang, L.; Zhu, L. LiNbO3-coated LiNi0.8Co0.1Mn0.1O2 cathode with high discharge capacity and rate performance for all-solid-state lithium battery. *J. Energy Chem.* **2020**, *40*, 39−45.

https://dx.doi.org/10.1021/acsenergylett.0c00040
ACS Energy Lett. 2020, 5, 955−961